Wintertime Spatial Distribution of Ammonia and its Emission Sources in the Great Salt Lake Region

Alexander Moravek[1], Jennifer G. Murphy[1], Amy Hrdina[1], John C. Lin[2], Christopher Pennell[3], Alessandro Franchin[4,5], Ann M. Middlebrook[5], Dorothy L. Fibiger[4,5*], Caroline C. Womack[4,5], Erin E. McDuffie[4,5,6**], Randal Martin[7], Kori Moore[7***], Munkhbayar Baasandorj[2,3], and Steven S. Brown[5,6]

[1]Department of Chemistry, University of Toronto, Toronto, ON, M5S 3H6, Canada
[2]Department of Atmospheric Sciences, University of Utah, Salt Lake City, UT, 84112, USA
[3]Division of Air Quality, Utah Department of Environmental Quality, Salt Lake City, UT, 84114, USA
[4]Cooperative Institute for Research in Environmental Sciences (CIRES), University of Colorado, Boulder, CO, 80309, USA
[5]NOAA Earth System Research Laboratory (ESRL) Chemical Sciences Division, Boulder, CO, 80305, USA
[6]Department of Chemistry, University of Colorado, Boulder, CO, 80309, USA
[7]Department of Civil and Environmental Engineering, Utah State University, Logan, UT, 84322, USA

[*]Now at California Air Resources Board, Sacramento, CA, 95814, USA
[**]Now at Department of Physics and Atmospheric Science, Dalhousie University, Halifax, NS, B2H 4R2, Canada
[***]Now at Space Dynamics Laboratory, Logan, UT, 84341, USA

Correspondence to: Alexander Moravek (a.moravek@utoronto.ca)

Abstract

Ammonium-containing aerosols are a major component of winter time air pollution in many densely populated regions around the world. Especially in mountain basins, the formation of persistent cold air pool (PCAP) periods can enhance particulate matter with diameters less than 2.5 μm ($PM_{2.5}$) to levels above air quality standards. Under these conditions, $PM_{2.5}$ in the Great Salt Lake Region of northern Utah has been shown to be primarily composed of ammonium nitrate, however, its formation processes and sources of its precursors are not fully understood. Hence, it is key to understand the emission sources of its gas-phase precursor, ammonia (NH_3). To investigate the formation of ammonium nitrate, a suite of trace gases and aerosol composition were sampled from the NOAA Twin Otter aircraft during the Utah Winter Fine Particulate Study (UWFPS) in January and February 2017. NH_3 was measured using a Quantum Cascade Tunable Infrared Laser Differential Absorption Spectrometer (QC-TILDAS), while aerosol composition, including particulate ammonium (pNH_4), was measured with an aerosol mass spectrometer (AMS). The origin of the sampled air masses was investigated using the Stochastic Time-Inverted Lagrangian Transport (STILT) model and combined with an NH_3 emission inventory to obtain model-predicted NH_x (= NH_3 + pNH_4) enhancements. Comparison of these NH_x enhancements with measured NH_x from the Twin Otter shows that modelled values are a factor of 1.6 to 4.4 lower for the three major valleys in the region. Among these, the underestimation is largest for Cache Valley, an area with intensive agricultural activities. We find that one explanation for the underestimation of wintertime emissions may be the seasonality factors applied to NH_3 emissions from livestock. An investigation of inter-valley exchange

revealed that transport of NH_3 between major valleys was limited and $PM_{2.5}$ in Salt Lake Valley (the most densely populated area in Utah) was not significantly impacted by NH_3 from the agricultural areas in Cache Valley. We found that in Salt Lake Valley around two thirds of NH_x originated within the valley, while about 30 % originated from mobile source and 60 % from area source emissions in the region. For Cache Valley, a large fraction of NO_x potentially leading to $PM_{2.5}$ formation may not

5   be locally emitted but mixed in from other counties.

1 Introduction

Ammonia (NH_3) is a key atmospheric pollutant, with significant impacts on air quality, climate, and ecosystem nitrogen availability. As the most abundant base in the atmosphere, NH_3 is an important precursor gas for secondary aerosol particle formation. As a result, ammonium-containing aerosols may comprise a significant amount of the particulate matter with a

10   diameter of 2.5 µm or less ($PM_{2.5}$) (Pozzer et al., 2017). High levels of $PM_{2.5}$ impact human health by increasing the risk for stroke, heart disease, lung cancer, and both chronic and acute cause respiratory deceases (WHO, 2016). Especially in urban areas, where a mix of pollutants such as nitrogen oxides (NO_x), sulfur dioxide (SO_2) or volatile organic compounds (VOCs) are present in elevated concentrations alongside NH_3, ammonium-containing aerosol can be a major source of $PM_{2.5}$. For example, NH_3 emitted from agricultural activities may be transported towards NO_x-rich urban centres to form ammonium

15   nitrate (NH_4NO_3) or ammonium sulfate ((NH_4)$_2SO_4$) aerosols (e.g., Zhao et al., 2017). This illustrates the importance of the transport and meteorological conditions in mixing the precursors that lead to secondary particle formation.

During the winter season, cold temperatures in combination with high pressure systems result in shallow boundary layers that trap and promote the build-up of pollutants near the surface, leading to enhanced secondary aerosol formation and winter smog. Periods with strong atmospheric stability are referred to as persistent cool air pool (PCAP) periods (Whiteman et al., 2014),

20   typically featuring a temperature inversion below the height of the surrounding terrain. In addition, the topography of mountain basins promotes the evolution of strong PCAP periods and thereby the confinement of pollutants near the surface. Under these conditions, urban areas such as Salt Lake City frequently experience high $PM_{2.5}$ concentrations. In the Great Salt Lake Region in northern Utah, the 24-hr U.S. National Ambient Air Quality Standard (NAAQS) for $PM_{2.5}$ (35 µg m^{-3}) is exceeded on average 18 days per winter (Silcox et al., 2012; Whiteman et al., 2014). Previous measurements made in the Salt Lake Valley

25   (Kelly et al., 2013; Kuprov et al., 2014) and recently published analysis of the UWFPS aerosol composition (Franchin et al., 2018) agree that during PCAP periods up to 75% of wintertime $PM_{2.5}$ is ammonium nitrate.

To develop appropriate $PM_{2.5}$ mitigation strategies in such areas where ammonium nitrate is high, it is essential to understand the mechanisms of local ammonium nitrate formation as well as the emission source of its precursor gases NO_x and NH_3. While emissions of NO_x are regulated, NH_3 is not regulated as a criteria air pollutant (CAP) in the U.S. As a consequence,

30   NH_3 emissions are not reported by NH_3 emitting industries or sectors to the same extent as other CAPs, resulting in higher

uncertainties of NH_3 emission estimates. In addition, observational networks for NH_3 are sparse compared to those for NO_x, which is in part related to the challenges in the measurement of NH_3. Therefore, improving the understanding of NH_3 sources is key to making reliable predictions of ammonium-aerosol formation and finding the appropriate mitigation strategies for $PM_{2.5}$.

5 To understand the sources of NH_3 in the Great Salt Lake Region, which are responsible for ammonium-aerosol formation and high levels of $PM_{2.5}$ in winter, we studied the spatial distribution of NH_3 in the three mountain basins as part of the Utah Winter Fine Particulate Study (UWFPS) (UWFPS report, 2018). The spatial distribution of NH_3 was measured from a Twin Otter aircraft and compared to NH_3 measurements from several ground stations in the region. The main objectives of this study are to identify the sources of NH_3 and the key emission sectors contributing to the regional formation of ammonium-aerosol. To

10 address these objectives, airborne measurements were compared to emission inventory-based NH_3 estimates. A footprint approach based on the Stochastic Time-Inverted Lagrangian Transport (STILT) model was used to estimate contributions from NH_3 source regions, while the results are discussed for the three major valleys in the study region. Finally, the exchange of air masses between valleys is investigated and discussed in respect to its role for ammonium-aerosol formation in the region.

2 Methods

15 **2.1 Study area and the Utah Winter Fine Particulate Study (UWFPS)**

The Utah Winter Fine Particulate Study (UWFPS) was carried out in January and February 2017 in the Great Salt Lake Region. The Great Salt Lake Region is located in northern Utah in the U.S. Western Rocky Mountains, comprised of three major mountain valleys (Salt Lake Valley, Utah Valley, and Cache Valley) and the Great Salt Lake (Fig. 1a). Salt Lake City, the most populated urban area in Utah and part of the Salt Lake City metropolitan area (1.2M inhabitants), is situated in the

20 northern part of Salt Lake Valley bordering the Great Salt Lake. Cache Valley (125k inhabitants), north of Salt Lake Valley, is separated by a branch of the Wasatch Range from the North Metropolitan Area and is characterized by its intensive agricultural activities, including concentrated animal feeding operations (CAFOs). The regulatory environment of Cache Valley straddles the states of Utah and Idaho and comes under the jurisdiction of two different US EPA regions (8 and 10). Utah Valley (575k inhabitants) borders Salt Lake Valley to the south via the Traverse Mountains and features Utah Lake, a

25 large freshwater lake in the valley centre, and agricultural and industrial activities, including a major gas-fuelled power plant. The objective of the UWFPS was to investigate wintertime air quality in the Salt Lake region, focusing on PCAP periods when formation of ammonium nitrate leads to high levels of $PM_{2.5}$. NOAA's Twin Otter aircraft flights and ground site observations in each valley were used to probe the spatial distribution of trace gases and aerosols, with the aim of identifying their importance for $PM_{2.5}$ and its formation mechanisms. A further objective of UWFPS was to investigate key emission sources

30 of aerosol precursors and the role of agricultural, industrial, urban, mobile, home heating and natural emission sectors.

From 16 January to 12 February 2018 a total of 23 research flights were carried out with the Twin Otter aircraft. Flights were performed in a north and south flight pattern, where the north pattern covered the North Metropolitan area, Cache Valley, Bear Valley, the Great Salt Lake, Tooele Valley and the Northern part of Salt Lake Valley. The South leg mainly encompassed Salt Lake Valley and Utah Valley. Figure 1 shows the region and county boundaries as well as a typical distribution of NH_3 mixing

5 ratios measured from the aircraft. Measurements were taken from ground level at the Salt Lake International Airport (1288 m, 5225 ft) through 3800 m (12500 ft) a.s.l. when flying over inter-valley mountain ranges (Fig. S1b). The lowest cruising altitude was around 150 m (500 ft) above ground level. To probe vertical profiles near the surface, missed approaches were performed at seven different air fields throughout the region (Fig. S1b).

2.2 Airborne ammonia measurements

10 A continuous wave Quantum Cascade Tunable Infrared Laser Differential Absorption Spectrometer (QC-TILDAS, Aerodyne research Inc., MA) (Ellis et al., 2010) was employed on the Twin Otter aircraft for measurements of NH_3 (see Fig. 2). The instrument uses a multi-pass absorption cell (0.5 L, 76 m effective path length) which is purged with sample air to measure NH_3. Due to its fast time response and high precision compared to other commercially available NH_3 analyzers, the instrument is suited for aircraft measurements (Hacker et al., 2016). Prior to installation on the Twin Otter, the weight of the single laser

15 instrument (QC-mini) was further reduced by using a smaller vacuum pump (SH-110, Varian Inc., MA) for generating the sample flow rate. The 4 L min^{-1} flow rate through the sample cell was set by the critical orifice of a PFA (Teflon) virtual impactor, which acted as a particulate matter filter to avoid interferences from thermally dissociated ammonium aerosol and also to protect the cell mirrors. That thermal dissociation of ammonium aerosol was negligible is shown by measurement periods where NH_3 was within the instrument's detection limit despite high levels (> 20 ppbv) of measured particulate

20 ammonium. As adsorption and desorption processes within the inlet system are major challenges for NH_3 measurements, the time response of the system was optimized by introducing an additional bypass flow rate of 16 L min^{-1} to purge the inlet line (PFA, 3/8" OD). The winglet that housed the inlet tubing was mounted directly above the QC-TILDAS allowing an inlet length of only 0.5 m. To further, minimize adsorption and desorption effects of NH_3 and humidity to the tubing wall, the winglet was heated to 40°C.

25 Variations in pressure, temperature and instrument vibrations may significantly impact the instrument performance by influencing the absorption spectrum fringe pattern. Fringes are periodic structures in the absorption spectrum which are caused by optical interferences within the laser beam path and can be responsible for signal drift if their pattern changes over time. To account for changing ambient pressures with flight altitude, a pressure controller (PC3P, Alicat Scientific Inc., AZ) was installed downstream of the absorption cell, which was able to keep the cell pressure at a constant value between 36.5 and 38.5

30 Torr. Inflight background measurements were performed manually approximately every 5 to 15 min to account for potential instrument drifts using zero air from an ultra-zero air cylinders.

The precision of the instrument during the campaign was significantly degraded from its usual performance due to difficulties with the laser source. As a result, NH_3 absorption was detected at 965.3 cm^{-1} instead of using the stronger absorption line at 967.3 cm^{-1}. A measurement precision at 1 Hz sample frequency of 150 pptv (1σ) could be achieved, which is similar to the background noise (200 pptv) of a QC-TILDAS that was operated by Hacker et al. (2016) on a different aircraft. Accordingly, the limit of detection (3σ) was 450 pptv at 1 Hz and 90 pptv for a 30 s averaging interval. Due to the effect of increased gravitational forces and vibrations on the optical alignment, data during take-off, landings and spiralling ascents and descents were not used in this study.

2.3 Airborne measurements of other trace gases and aerosols

The Twin Otter aircraft was equipped with an Aerosol Mass Spectrometer (AMS, Aerodyne Research Inc., MA) to measure the chemical composition of the non-refractory aerosol particles in the 70 to 800 nm range (NR-PM1) (Drewnick et al., 2005; Jayne et al., 2000) . The operation of the AMS during UWFPS is described in detail in Franchin et al. (2018). In brief, ambient aerosol particles are focused in an aerodynamic lens, evaporated, ionized with electron-impact ionization and detected by a mass spectrometer. The AMS measured mass loadings of particulate nitrate (pNO_3), ammonium (pNH_4), organic species, sulfate (pSO_4), chloride (pCl), and total aerosol mass, with detection limits of 0.04, 0.09, 0.33, 0.03, 0.07, and 0.38 $\mu g\ m^{-3}$ respectively. The uncertainty on the total AMS mass concentrations is estimated to be 20% (Bahreini et al., 2008). Aerosol mass with the AMS was well-correlated with aerosol volume measured with an Ultra High-Sensitivity Aerosol Spectrometer (UHSAS, Droplet Measurement Technologies, CO) on the same sampling line as the AMS.

Nitrogen oxides ($NO_x = NO + NO_2$), total reactive nitrogen (NO_y) and ozone (O_3) were measured at 1 Hz using the NOAA nitrogen oxides cavity ringdown instrument (NOxCaRD). The instrument measures NO_2 directly by optical absorption at 405 nm, while NO and O_3 are measured in two separate channels after quantitative conversion to NO_2 by reaction with excess O_3 or NO, respectively (Fuchs et al., 2009; Washenfelder et al., 2011). A fourth channel measures NO_y by conversion to NO and NO_2 in a heated quartz inlet (650 °C) and subsequent conversion of NO to NO_2 in excess O_3 (Wild et al., 2014). Accuracies for NO_x, NO_2 and O_3 were 5% and 12% for NO_y, based on previous comparison of the NO_y measurement to a standard NO_y instrument (Wild et al., 2014)..

A commercial probe (Avantech) measured meteorological parameters (ambient temperature, pressure, relative humidity with respect to liquid water, wind speed, and wind direction), the global positioning satellite (GPS) location including altitude above sea level, and aircraft parameters (heading, pitch, and roll). Wind data were compromised for some flights, making only partial coverage available. The aircraft GPS altitude above sea level was converted into altitude above ground level using USGS data (https://gis.utah.gov/data/elevation-and-terrain/).

2.4 Ground site observations

During UWFPS, a series of ground measurements were conducted to measure the evolution of trace gases, aerosols and meteorology during the pollution episodes in the study region. Data used in this study were taken from the University of Utah ground site (UU) in Salt Lake Valley (40.7663, -111.8477), the Logan ground site (L4) in Cache Valley (41.7589, -111.8151) and the North Provo ground site (NP) in Utah Valley (40.2528, -111.6627) (Fig. 1c). The Logan ground site is referred to as L4 as it is located approximately 3 km north east from the actual downtown federal reference site (named L4).

The UU site is located on the top floor of William Browning Building on the University of Utah campus, which is situated on the north east side of the Salt Lake Valley, and approximately 150 m above the valley floor. A sampling inlet was located on top of a 7 m observation tower, at a height of 40 m a.g.l. Online measurements of ambient air $PM_{2.5}$ composition and gas phase precursors were performed using University of Toronto's modified Ambient Ion Monitoring System (AIM 9000D, URG Corp., NC) coupled with two ion chromatographs (Dionex ICS-2000, Thermo Fisher Scientific, ON). The system measures water soluble gases (NH_3, SO_2, HNO_3) and particles (pNH_4, pSO_4, pNO_3) at an hourly resolution using parallel wet denuders (Markovic et al., 2012). Continuous $PM_{2.5}$ mass concentrations were determined using the 8500 Filter Dynamics Measurement System (FDMS) coupled with a TEOM 1400ab ambient particulate monitor. Instrumental background measurements were conducted by introducing an overflow of zero air into the AIM-IC inlet and sampled for a 24-hr period. Based on background experiments, the 3σ detection limits were determined to be 0.15 ppb for NH_3 and 0.3 µg m^{-3} (at STP) for pNH_4.

The L4 ground site was a temporary sampling station during UWFPS, located on the Utah State University campus in Logan, employing an environmentally controlled shelter with the inlet extending through the shelter roof to a height of 5 m a.g.l. Ambient mixing ratios of NH_3 were obtained with a Picarro G2508 cavity-ringdown spectroscopy instrument (Picarro Inc., CA). The analyzer collected on a nominal 5 s sampling frequency, which is averaged up to 1 min sample periods. At one minute averaging times the G2508 has a precision of <3 ppbv and measured detection limit (3σ) of 2.3 ppb. A Teledyne API T640 measured continuous mass concentrations of $PM_{2.5}$, PM_{10}, and $PM_{10-2.5}$ at the L4 ground site.

At the NP site, mass concentration of $PM_{2.5}$ was monitored by the Utah Division of Air Quality using a 1405-DF TEOM Continuous Dichotomous Ambient Air Monitor (Thermo Fisher Scientific Inc., MA). No NH_3 measurements were available from this site.

2.5 The UDAQ emission inventory

To better understand the formation of ammonium nitrate in the study region, it is important to identify and quantify the major sources of NH_3. In northern Utah, NH_3 from livestock, fertilizer and on-road vehicle emissions are the most dominant NH_3 sources, according to the emission inventory provided by the Utah Division of Air Quality (UDAQ). The Utah emissions inventory is created by UDAQ and ultimately informs the emissions estimates found in the U.S Environmental Protection

Agency's (EPA) National Emission Inventory (NEI). Yearly totals of county-wide emission data for criteria and other significant air pollutants (NO_x, VOC, direct PM_{10}, direct $PM_{2.5}$, NH_3, SO_2, CO, and others) are processed in the SMOKE v3.6.5 (Sparse Matrix Operator Kernel Emissions) emissions processing software to obtain higher temporally and spatially resolved emission estimates (Baek and Seppanen, 2018). UDAQ uses two modelling domains: (1) a larger 4 km resolution outer-domain

5   covering the State of Utah and portions of surrounding states and (2) a smaller 1.33 km inner-domain covering the Wasatch Range and Cache Valley, representing the majority of the $PM_{2.5}$ non-attainment area in northern Utah. Temporal allocation in SMOKE consists of defining emission distributions through the use of monthly, weekly and hourly profiles, which are applied to the yearly emission totals.

Inventory data are compiled for four distinct emission sectors: area, non-road, mobile and point sources. Total estimated daily

10   NH_3 emissions from each sector are given in Table 1 for the regions in the study area. NH_3 emissions in all regions are dominated by areas sources with the exception of Salt Lake Valley, where NH_3 from mobile sources are thought to be dominant. Area sources include NH_3 emissions from fertilizer applications, livestock and residential wood combustion. Emissions from livestock are the largest portion of area sources in Utah County (71%) and Cache County (81%), while they are only minor in Salt Lake County (11%). The NEI-based NH_3 emissions from livestock are based on county-level animal populations, which

15   are multiplied by daily-resolved emission factors that are representative for each animal type and management practice. These location-specific emission factors are produced by a Farm Emission Model (FEM) for each day of the modelled year by taking meteorological as well as animal type and practice input data (McQuilling and Adams, 2015). For the compilation of NH_3 emissions from fertilizer applications, a bi-directional exchange model uses meteorological and application-based input data. The Environmental Policy Integrated Climate (EPIC) modelling system provides information regarding fertilizer timing,

20   composition, application method, and amount. A bidirectional version of the Community Multiscale Air Quality (CMAQ) is then used to calculate county-level emission factors which are multiplied by county-level total fertilizer estimates to obtain NH_3 emissions. For both, livestock and fertilizer NH_3 emissions annual NEI emission totals are multiplied in SMOKE by monthly, weekly and hourly profiles.

Non-road emissions include emissions from non-stationary sources, except commuter automobiles. For example, non-road

25   sources would include construction equipment, snowmobiles, boats, trains, and aircraft. Similar to mobile emissions, non-road emissions are mainly projected using the MOVES 2014a model. However, the emissions from trains, aircraft, and airport ground support equipment are estimated from specific EPA-provided tools.

Mobile emissions are calculated and projected using the MOVES 2014a model, which are then input into SMOKE as precomputed mobile inventory numbers. Mobile emissions are informed by vehicle population data and vehicle-specific

30   emissions-rate information. Also, various metropolitan planning organizations supply UDAQ with the traffic activity data that goes into MOVES 2014a.

Point sources include large emitters such as oil refineries, power plants, and big mining operations. Since the vertical release height of point stack emissions impact air quality, the 2D SMOKE gridded emissions output is input into the air-quality model (CAMx 6.30), which calculates vertical plume rise from those point source stack parameters using 42 layers matching WRF inputs.

2.6 Modelling of ammonia concentrations using STILT

To account for the atmospheric transport of NH_3 from emission sources to the receptors of the NH_3 measurement observations made during UWFPS, we used the Stochastic Time-Inverted Lagrangian Transport (STILT) model (Lin et al., 2003). STILT simulated the upstream influence by modelling the evolution of ensembles of 200 simulation particles, each representing an air parcel 24 hours back in time. Particle ensembles are considered to be influenced by surface fluxes when they spend time in the vertically well-mixed surface layer (defined as 50% of the boundary layer height). STILT compiles a "footprint", a flux sensitivity matrix, using the flux sensitivity from each of the 200 trajectories. The flux sensitivity represents the contribution of a grid cell area to the NH_3 mixing ratio per surface flux unit. To obtain footprints for the aircraft measurements, STILT was run for every 2 min of the Twin Otter flight path for all 23 research flights. STILT was driven with gridded meteorological information available from NOAA's High Resolution Rapid Refresh (HRRR) model (http://ruc.noaa.gov/hrrr/), which covers the entire continental U.S.. HRRR is based upon the widely-used Weather Research and Forecasting (WRF) mesoscale model (Skamarock and Klemp, 2008) and resolves the atmosphere at 3-km grid spacing, assimilating radar observations.

Model NH_3 enhancements (in pptv) were estimated by multiplying the flux sensitivity data (in pptv/(μmol m^{-2} s^{-1})) with the NH_3 emissions from the UDAQ emission inventory (in μmol m^{-2} s^{-1}) for each grid cell. As STILT was run 24 hrs back in time, the modelled NH_3 enhancements represent the NH_3 mixing ratio contribution from surface emissions within the last 24 hrs. Before multiplying, the NH_3 emissions were resampled to the match the spatial grid of the flux sensitivity data (0.01° x 0.01°). Modelled NH_3 enhancements were then obtained by summing the NH_3 contributions from each grid cell. To account for the large spatial extent of the 24-hr trajectories from the Twin Otter position, the 1.33 km inventory data was inset into the larger 4 km inventory, to have the maximal spatial extent but also make use of the refined NH_3 emissions of the 1.33 km emission inventory.

To account for formation of particle ammonium from emitted NH_3, the modelled NH_3 estimates are compared to measured total NH_x (= NH_3 + pNH_4). Conversion to particulate ammonium is the dominant reactive sink for gas phase NH_3 as the oxidation of NH_3 by OH is significantly slower. Thus using NH_x as a passive tracer is reasonable, however, the approach does not account for potential dry and wet deposition of NH_3. As a result of this simplification, modelled NH_x enhancements could be overestimated. Modelled NH_x enhancements only account for NH_3 emitted within the past 24 hr in the spatial domain of the produced NH_3 contributions map and do not include NH_x advected from outside that spatial domain or NH_3 which was present in the air shed before the 24 hr period. Therefore, an estimate of background NH_x mixing ratios was subtracted from

measured NH_x mixing ratios before comparing them to the modelled enhancements. Background mixing ratios were determined separately for each region listed in Sect 2.1 (see Fig. 1a), using the measured NH_x mixing ratios data from each individual flight in the respective region. To account for varying vertical mixing between flights, the data were split into vertical layers of 50 m depth covering the entire altitude range of the Twin Otter. The background mixing value specific for

5   each layer, region and flight was then determined by the 1st percentile of NH_x data from the Twin Otter. As shown in Fig. S14, for areas with significant NH_3 surface emissions, the 1st percentile was well above the instrument's detection limit. If the background mixing ratio was underestimated, this would lead to unrealistically high estimates of the NH_x enhancements from the measurements.

In the remainder of the text, we refer to modelled NH_3 and measured NH_x enhancements as modelled and measured dNH_x,
10   respectively.

3 Results and discussion

3.1 Meteorological conditions and PCAP episodes

Weather conditions in the Great Salt Lake Region in January and February 2017 included episodes of winter storms and above-average precipitation. As storm tracks promote vertical mixing, PCAP periods were less frequent during UWFPS than typically
15   observed. Within the period of the Twin Otter measurements, two major PCAP periods were identified: PCAP#1 from 13 to 20 January 2017 and PCAP#2 from 27 January to 4 February 2017. A third and less intense PCAP period occurred at the end of the campaign on 13 February and lasted until 18 February 2017. The strong atmospheric stability during those PCAP periods lead to the build-up of high $PM_{2.5}$-levels for Salt Lake Valley, Cache Valley and Utah Valley, as shown in Fig. 3. Due to the lack of snow cover and the relatively weak subsidence inversion, the inversion height during PCAP#1 was atypically high,
20   reaching from about 400 m up to 800 m a.g.l., before a strong storm initiated the top-down erosion of the PCAP on 19 January. During PCAP#1, ground-level $PM_{2.5}$ reached up to 90 µg m^{-3} in Cache Valley (L4), and up to 50 µg m^{-3} in Salt Lake Valley (UU), while the PCAP was only weakly developed in Utah Valley (NP) with $PM_{2.5}$ levels below 20 µg m^{-3} (1-hr averages). In contrast, PCAP#2 was a stronger, classic PCAP period, which was promoted by several inches of fresh snow and cold air left by a storm that was followed by a large high pressure period. This resulted in $PM_{2.5}$ values building up in all three major
25   valleys over the course of the PCAP and reaching 104 µg m^{-3} at the L4, 64 µg m^{-3} at the UU, and 80 µg m^{-3} at the NP sites (1-hr averages). As evident in the $PM_{2.5}$ data, the PCAP started eroding in Utah Valley first, then in Salt Lake Valley second, whereas it persisted a few days longer in Cache Valley, which is also attributed to the deeper snow cover in Cache Valley during January and February 2017. Compared to PCAP#2, PCAP#3 was moderate with only the onset captured by the aircraft flights.

3.2 Observed NH$_3$ mixing ratios

3.2.1 Evolution of ammonia mixing ratios near the surface

Ammonia mixing ratios measured at the L4 and UU ground sites (Fig. 3), correlate with increasing PM$_{2.5}$ levels during PCAP periods, especially at the L4 site (Fig. 3a), where NH$_3$ reached up to 100 ppbv during PCAP#1 and PCAP#2. The correlation

5 between PM$_{2.5}$ and NH$_3$ indicates the presence of local NH$_3$ sources, and illustrates the strong influence of atmospheric stability on pollutant concentrations during winter. NH$_3$ mixing ratios show a stronger diurnal variation than PM$_{2.5}$. Accumulation of directly emitted NH$_3$ in the nocturnal boundary layer leads to transient enhancements of NH$_3$ mixing ratios, which is for example visible in the short-term (<12 hrs) NH$_3$ peaks observed during night time at the L4 site (e.g. nights of 08/09 and 09/10 February). Although PM$_{2.5}$ formation occurs through both daytime and night-time processes, the nigh-time process is typically

10 fast in the residual layer and suppressed in the surface layer (McDuffie et al., 2019; Womack et al., 2019). At the UU site, ambient NH$_3$ measurements were significantly lower than in Cache Valley, typically below 10 ppbv (Fig. 3b). Measurements are not available for PCAP#1, however, the build-up of NH$_3$ mixing ratios in Salt Lake Valley is evident in the second half of PCAP#2. Increasing PM$_{2.5}$ levels mark the first half of PCAP#2, while NH$_3$ mixing ratios were still low between 1 and 3 ppbv. During that period, NH$_3$ mainly partitioned into pNH$_4$ as it was observed by the simultaneous increase of pNH$_4$ with PM$_{2.5}$

15 (data not shown).

Near surface mixing ratios were sampled from the Twin Otter aircraft during missed approaches at regional airfields (Fig. S1 and S2). Figure 3a shows NH$_3$ mixing ratios at Logan airport, located about 3 km northwest of the L4 ground site. NH$_3$ mixing ratios from the Twin Otter follow the trend of the ground measurements with (1) high mixing ratios between 45 and 55 ppbv during PCAP#1, (2) medium mixing ratio levels between 20 and 25 ppbv during the first half of PCAP#2, and (3) lower mixing

20 ratios below 20 ppbv towards the end of the measurement campaign. The direct comparison of ground site and Twin Otter measurements was performed by averaging the Twin Otter mixing ratios within a distance of 1 km of the airport runway and obtaining the mean ground site mixing ratios for the same time interval. As shown in Fig. S3b, mean values from the Twin Otter are roughly a factor of two lower than measurements from the L4 ground site. This can be explained by dilution of NH$_3$ mixing ratios from higher altitudes as the averaging window for the Twin Otter values partially includes NH$_3$ measurements

25 from the ascents and descents of the missed approaches. For that reason, maximum values better represent the ground level mixing ratios, which is supported by a closer correspondence with the data from the L4 site. Furthermore, Moore (2007) and Hammond et al. (2017) showed that mean NH$_3$ concentrations can vary spatially across the Cache Valley by as much as an order of magnitude, depending on the strength of adjacent sources and duration of a PCAP event. For Salt Lake Valley, NH$_3$ measured at the UU site compares generally well with the airborne NH$_3$ obtained when the Twin Otter was overflying the

30 ground site (Fig. 3b). The direct comparison of both measurements (Fig. S3a) shows that airborne measurements are on average lower, attributed to the higher altitude of the measurement and the vertical gradient of NH$_3$ away from the surface.

3.2.2 Prevailing NH_3 mixing ratios in different regions from aircraft observations

The frequency distributions of NH_3 mixing ratios measured in Salt Lake Valley, Cache Valley, Utah Valley and over the Great Salt Lake are shown in Fig. 4a and 4b for both PCAP and non-PCAP conditions. Mixing ratios were filtered to only include those from the lowest steady flight level (data between 100 – 500 m a.g.l) for a better comparison between regions. The histograms reveal that during both PCAP and non-PCAP conditions NH_3 mixing above the Great Salt Lake were mostly below 3 ppbv and in Salt Lake Valley mostly below 5 ppbv, with only a few measurements outside of those limits. The majority of NH_3 measurements in both Cache Valley and Utah Valley were also below 5 ppbv, however, higher mixing ratios up to 20 ppbv in Cache Valley and 10 ppbv in Utah Valley were also frequently observed. While the distributions for all regions are similar under PCAP and non-PCAP conditions, during PCAP conditions higher extreme values up to around 70 ppbv in both Cache Valley and Utah Valley were observed at the lowest steady flight level, indicating the presence of local emission sources. Higher levels up to nearly 90 ppbv were only measured during missed approaches at the Logan airport in Cache Valley, marking it as a distinct high NH_3 region. In contrast to NH_3, the frequency distributions of pNH_4 show clear difference between PCAP and non-PCAP periods (Fig. 4c, d), with significantly higher pNH_4 values during PCAP conditions. This can be explained by increased partitioning of NH_3 into the particle phase and build-up of ammonium nitrate over the course of the PCAP periods (Fig. 3).

3.3 Evaluation of NH_3 emission sources

3.3.1 Comparison of modelled and measured enhancements

To investigate NH_3 emissions sources in the different regions, we compare dNH_x measured on the Twin Otter with dNH_x derived by the footprint model (see Sect. 2.5 and 2.6). Figure 5 shows an example of a STILT flux sensitivity footprint, and how it is overlaid with the UDAQ emission inventory to obtain dNH_x estimates for the locations of the Twin Otter.

The mean measured and modelled dNH_x for all regions in the study area are given in Table 1, including a scaling factor which is the ratio of dNH_x_meas/dNH_x_model. Figure 6 shows the frequency distribution for modelled and measured dNH_x for Salt Lake Valley, Cache Valley and Utah Valley for non-PCAP (a-c) and PCAP (d-f) conditions. The distributions show that the model underestimates dNH_x in all three valleys, compared to the measurements from the Twin Otter. During non-PCAP conditions, the underestimation is most prominent in Cache Valley. During PCAP conditions the underestimation is in general more pronounced than during non-PCAP conditions. As during PCAP periods NH_x mainly persists as pNH_4 (see Section 3.2.2), this leads to the high measured dNH_x over the course of the PCAP period in Salt Lake Valley and Utah Valley. Due to high local NH_3 emissions, in Cache Valley NH_3 and pNH_4 are of similar magnitude, which is why the difference between PCAP and non-PCAP periods is slightly less pronounced (see also linear scale distributions in Fig. S8).

Lower modelled dNH_x values may suggest an underestimation of NH_3 emissions in the UDAQ inventory. Table 1 lists the mean measured and modelled dNH_x mixing ratios for the different regions in the study area, which were used to derive a mean scaling factor between measured and modelled values. The mean scaling factor for Cache Valley, Salt Lake Valley and Utah Valley are 4.4, 1.9 and 1.6, respectively, which reflects that modelled dNH_x are underestimated in all three valleys. Due to the

5   non-Gaussian distribution of both measured and modelled dNH_x values, the median scaling factors vary but still show the same trend for underestimation of modelled dNH_x, with highest underestimation in Cache Valley (2.7), followed by Salt Lake Valley (1.9) and Utah Valley (1.2).

To further discuss the discrepancies between measured and modelled dNH_x values, it is important to address the uncertainties of both measured and modelled dNH_x, which we discuss in the following section.

10   **3.3.2**   **Uncertainties in measured and modelled mixing ratio enhancements**

Calculations of the trajectories and footprints with the STILT model rely on the accurate representation of meteorological conditions and parameterizations such as the definition of the height of the surface mixed layer, which couples the ground surface emissions to the calculated trajectories. While we do not go in detail on the STILT parameterization and the derived weather model (HRRR), the examination of NO_y enhancements above background mixing ratios (dNO_y), which were also

15   measured from the Twin Otter, gives confirmation that the overall representation of the meteorology is reasonable. Figures S12 and S13 show the frequency distributions for measured and modelled dNO_y. The scaling factors (dNO_y measured/dNO_y modelled) for Cache Valley, Salt Lake Valley and Utah Valley were 1.3, 1.0 and 0.9, respectively, which shows agreement of measured and modelled dNO_y for all of the three valleys. This indicates that on average both meteorological conditions and NO_y emissions are represented adequately in the model approach we used. This interpretation relies on the assumption that

20   both the NO_x emission inventory and NO_y measurements are accurate. As particulate nitrate (pNO_3) is only quantitatively sampled by the NOxCaRD if it enters the inlet (not designed specifically for aerosol sampling), NO_y measurements may be biased low. By comparing the NO_y to the AMS pNO_3 (after subtracting NO_x and other relevant NO_y species), we found that inlet sampling was effectively quantitative to within the uncertainty in the AMS (20%) and NO_y (12%) measurements. Furthermore, since the NO_x to NO_y ratio was always fairly large (0.53 ± 0.34), a significant amount of NO_y was present as

25   NO_x. While the agreement in the frequency distributions is good, the direct comparison of modelled and measured dNH_x reveals a relatively poor point-to-point correlation (Fig. S7). A similarly poor correlation was found for dNO_y (Fig. S11) and also for measured and modelled dNH_x, dNO_y and dCO_2 at the UU ground site (data not shown), which shows that there is no clear bias in either the STILT footprints from the Twin Otter or in the NH_3 inventory.

Due to the finite extent of the combined UDAQ emission inventory map (Sect. 2.5), fractions of the STILT footprints may be

30   outside of the emissions inventory domain. For both Salt Lake Valley and Utah Valley, more than 50% of the 24-hr footprints lie completely within the inventory domain during PCAP conditions, while only a small number that have a contribution from

outside of the domain of 50% or more. As Cache Valley is located close to the northern border of the UDAQ emission inventory map (Fig. 1), a larger fraction of footprints exceeded the inventory domain, with 18% of footprints completely within the inventory domain and 63% of footprints at least 50% within the domain during PCAP conditions. However, this effect cannot explain the large underestimation of modelled dNH_x in Cache Valley due to the following reasons: (1) the analysis of the

5   STILT trajectories (Fig. S15) showed that air masses for a majority of the extreme measured dNH_x values in Cache Valley originated in low NH_x environments (at high altitudes or areas with low NH_3 emissions), and (2) high mixing ratios were only observed in Cache Valley (see also Fig. 4), providing evidence that measured dNH_x were dominated by local NH_3 sources. Advection of high amounts of NH_3 from the north would have also strongly affected other regions such as the Great Salt Lake, which the measurements do not show.

10 Uncertainties of measured dNH_x values arise from uncertainties in the measurements from the Twin Otter and uncertainties in the background determination (Sect. 2.2 and 2.3). The precision of NH_3 mixing ratios was 0.09 ppbv for a 1 min averaging period, which was used for the comparison. The uncertainty of pNH_4 is given as 20%. Given the uncertainty in the measurements and an uncertainty of the background determination method, the distinction between small measured and modelled dNH_x differences is difficult. As a result, although the scaling factors in Table 1 suggest that NH_3 emissions in Salt

15 Lake Valley are underestimated by 50%, it is possible that part or all of the model-measurement mismatch could be due to method uncertainties rather than due to an underrepresentation of NH_3 emission in the UDAQ inventory. In contrast, the large differences between measured and modelled dNH_x in Cache Valley, cannot be attributed to measurement errors, and therefore is more likely attributed to an underestimation of NH_3 emission in the UDAQ inventory in Cache Valley.

3.3.3 Modification of modelled dNH_x using scaling factors

20 To investigate the effect of a possible underestimation of NH_3 emissions in the UDAQ inventory on the presented dNH_x distributions, we scaled the modelled dNH_x by the scaling factors given in Table 1. For Cache Valley, if we assume that all the underestimation in modelled dNH_x is due to an underestimation in livestock emissions (see Sect. 3.3.4), we can adjust the scaling factors in Table 1 to be solely applied to area source emissions. Accordingly, the area source scaling factor for Cache Valley is 4.55. If we apply this factor to the modelled dNH_x in Cache Valley, the range of measured and modelled dNH_x agrees

25 well for non-PCAP conditions (Fig. 7a). As the same factor is applied to all modelled dNH_x, the shape of distribution does not change significantly, and a much larger scaling factor would be necessary to reproduce measured dNH_x values up to 88 ppbv for the PCAP conditions (Fig. 7c). A Mann-Whitney-Wilcoxon test was used to evaluate the agreement between modelled and measured dNH_x distribution before and after applying the scaling factor (Table S2). The increase of p-values above the 0.05 significance level indicates that the distributions of modelled and measured dNH_x show similarity after applying the scaling

30 factor. Assuming a systematic underestimation of livestock emissions, we applied the same scaling factor also to area source emissions in Salt Lake Valley and Utah Valley. As illustrated in Fig. S9, for Salt Lake Valley the modified modelled dNH_x

are not significantly larger, which is due to the fact that emissions from area sources play a less important role in Salt Lake Valley than in Cache or Utah Valley (Table 1). Since the largest emissions source in Salt Lake Valley is the mobile sector, modelled dNH_x for all three valleys were additionally modified by a scaling factor, which was retrieved from the ratio of modelled and measured dNH_x value in Salt Lake Valley (Fig. S10). Applying the factor (= 3) to the mobile emissions of

5   modelled dNH_x, yields a better agreement for Salt Lake Valley during non-PCAP conditions, however, the large frequency of measured dNH_x above 10 ppbv during PCAP conditions cannot be explained. This suggests that especially during PCAP conditions either (1) background NH_x mixing ratios used to calculate measured dNH_x are higher than accounted for or (2) the surface influence in STILT is underestimated in Salt Lake Valley.

3.3.4 Ammonia emissions in Cache Valley: Uncertainties in livestock emissions

10   The results presented above suggest that NH_3 emissions may be underestimated in the UDAQ emission inventory, with highest underestimation in Cache Valley. According to the inventory, 96.7% of total NH_3 emissions in Cache Valley are attributed to emissions from area sources. Cache Valley area sources are dominated by emissions from cattle waste (56.2%) and poultry operations (20.6%). Emissions from fertilizer application only account for 6.8% and from swine production only 3.1% of the total area sources. As cattle waste is by far the largest NH_3 source in Cache Valley, it therefore seems most likely that an

15   underrepresentation of cattle waste emissions are at least partially responsible for the gap between measured and modelled dNH_x.

In the UDAQ inventory, sources from livestock emissions are treated as areas sources and distributed uniformly over the county or an area in the county. As a result, high NH_3 emissions released by CAFOs are spread over a larger area instead of being treated as a point source. This may be another reason why the higher measured dNH_x values are not reproduced by the

20   model. As the UDAQ inventory does not report the location of CAFOs, we modelled dNH_x using a NH_3 emission inventory compiled by Utah State University (USU), which reports facility-based emissions from livestock in Cache Valley (see Section S4 for a description of the inventory). The USU inventory compiled emissions from dairy cattle, beef cattle, swine, poultry, automobiles, wastewater treatment facilities, and industry for both Cache and Franklin Counties for the year 2006 (Table S1). In winter time, the largest NH_3 emissions source in Cache Valley was dairy cattle (89.6%), while 98.1% of total emissions

25   were from the livestock sector. Figure S5 spatially locates the facility-based livestock, poultry and other area source NH_3 emissions in Cache Valley and visually indicates estimated relative source strengths. To derive modelled dNH_x estimates, we replaced the UDAQ NH_3 emissions in Cache Valley with these facility-based emissions from the USU inventory. These emissions were embedded into the UDAQ emission inventory map (Fig. S6) before overlaying them with the STILT footprints from the Twin Otter. Compared to the original UDAQ inventory, the USU inventory produces higher modelled dNH_x values,

30   which compare better to dNH_x measured from the Twin Otter. The USU emissions yield a mean modelled dNH_x value of 5.05 (± 8.38) ppbv, as shown in Table 1, whereas using the UDAQ inventory this value was only 1.70 (± 1.47) ppbv. Maximum

modelled dNH_x values from each inventory are 61.7 and 5.7 ppbv, respectively. Mean dNH_x mixing ratios from the USU are a factor of 2.55 higher than from the UDAQ inventory, which agrees with the ratio between total emission rates from each inventory in Cache Valley given in Table 1 (12435 kg d^{-1} ÷ 4757 kg d^{-1} = 2.61). In comparison to measured dNH_x, the scaling factor (all sectors included) decreases from 4.4 to only 1.5 when using the USU inventory.

5   Possible reasons for the underestimation of NH_3 emissions in the UDAQ inventory could be differences in the livestock numbers or differences in livestock emission factors used in the inventories. As described in Moore (2007), the USU inventory uses animal counts from 2007, derived from personal discussions with count extension agents, local producers and co-op organizations, with approximately 90,000 dairy cattle in Cache Valley (40,000 in Cache County; 50,000 in Franklin County) and nearly 2,000,000 chickens. The USU inventory is based on a NH_3 emission factor between 152.7 and 161.3 g d^{-1} AU^{-1}

10 (AU = animal units), depending on the cattle age and waste disposal method. Dairy cattle emissions in the UDAQ are based on the county wide estimates of the 2014v1 NEI inventory. As mentioned in Sect. 2.5, the FEM used in the NEI inventory produces location specific emission factors for each day of the modelled year (McQuilling and Adams, 2015). In SMOKE, annual NEI emission totals are multiplied by monthly, weekly, and hourly profiles to obtain temporally resolved emissions. The monthly profile redistributes the annual total NEI emissions over the year and is determined through inverse modelling,

15 as described in Gilliland et al. (2006). NH_x observational data from the National Atmospheric Deposition Program (NADP) is used together with prior seasonal NH_3 emission estimates in the CMAQ model to produce a region specific monthly profile. The monthly profile used in the UDAQ inventory is presented in Fig. S4 showing a clear seasonal cycle of livestock emissions. Emissions peak in summer, with more than 18% of annual emissions in July, while emission are lowest in wintertime. This seasonal profile is typically explained by increases in fertilizer application, a higher fraction of outdoor housing and higher

20 temperatures in summer than in winter. However, a significant month-to-month variation is present. Especially in wintertime, when expected emissions are lower, the percentage variation between months is significant. This suggests uncertainties in wintertime livestock emissions, in particular as the monthly profile is based on the year 2005. Furthermore, as shown in Table S1, the USU inventory suggests nearly similar livestock emissions for both summer and winter. This is supported by on average higher surface NH_3 concentrations observed in winter than summer in Cache Valley by the authors of the inventory in 2006

25 (Moore, 2007).

It is beyond the scope of this study to evaluate the uncertainties of inventory livestock emissions in detail. A larger measurement dataset and also a more thorough consideration of other processes such as NH_x deposition are necessary.

3.4 Inter-valley exchange of NH_3 and impact on PM formation

Exchange of air masses between valleys or basins in the study region can be a critical factor for air pollution formation.

30 Especially in wintertime when air pollutants accumulate in the valley basins during PCAP periods, the transport of air pollutants or their precursors from adjacent valleys can increase local air pollution. If NH_3 from agriculture in the Cache Valley

is transported to Salt Lake Valley, its equilibrium with HNO_3 produced from oxidation of NO_x emitted by mobile and industrial sources may affect the limiting reagent and thus the control strategy for ammonium nitrate $PM_{2.5}$ formation in Utah's most densely populated region (Franchin et al., 2018). Similarly, NO_x enriched air masses transported from Salt Lake Valley may lead to $PM_{2.5}$ formation in Cache Valley. Utah Valley is connected with Salt Lake Valley via the Jordan Narrows, where

5 exchange of air masses between the two basins is frequently observed. For example, after a mix-out episode at the end of a PCAP period in Salt Lake Valley, Mitchell et al. (2018) observed the transport of $PM_{2.5}$ enriched air from Utah Valley, where the PCAP was still persistent. Similarly, we observed from the Twin Otter the transport of NH_3 rich air masses through the Jordan Narrows into Salt Lake Valley, induced by southerly winds during PCAP#1 on 18 January 2017 (mixing ratios in Utah Valley and Salt Lake Valley for that day are shown in Fig. 1c).

10 To investigate how inter-valley exchange affects air pollution in the Great Salt Lake Region, we examined the origin of air masses through the STILT footprint calculation. The dNH_x contribution from each county to the modelled total dNH_x was determined for the Twin Otter footprints by using emissions from the UDAQ inventory. In addition we, determined the county contribution to dNH_x at the UU site, where hourly STILT emission enhancements were available for the period from 16 to 31 January 2017. Due to the lower elevation of the ground-based UU site compared to the Twin Otter aircraft, the extent of the

15 footprints is typically smaller; however, footprints for UU provide more continuous temporal coverage over the investigated period.

Figure 8a shows the dNH_x contributions for Salt Lake Valley (UU site and Twin Otter), Cache Valley (Twin Otter), and Utah Valley (Twin Otter). Results for the other regions in the study area are presented in Fig. S16. The contributions were segregated by county (e.g. Salt Lake County instead of Salt Lake Valley) as political boundaries are more appropriate divisions for

20 emission control and air pollution regulation. In Salt Lake Valley, the largest portion of dNH_x at the UU site is attributed to emissions from Salt Lake County for both PCAP (66.3%) and non-PCAP (77.2%) conditions. As Twin Otter footprints extend further than those from surface observations, contributions from Salt Lake County NH_3 are slightly smaller (47.6 and 40.8%). The second largest contributions are from Davis County adjoining to the North of Salt Lake Valley (13.0 and 24.2% for Twin Otter). Contributions from Utah County are small at the UU site (8.2 and 3.7%), but (16.9%) for the Twin Otter-derived

25 footprints during PCAP periods, as the aircraft also sampled the south section of Salt Lake Valley. This is consistent with frequently observed southerly winds during PCAP periods and shows the importance of inter-valley exchange during these conditions. Contributions from Cache County were only minor (0.5 and 0.0% at UU site, 2.6 and 6.5% for Twin Otter over SLV) and negligible from Franklin County (0.0% at UU site, 0.1 and 1.7% for Twin Otter over SLV). This shows that the impact of the high agricultural emissions in Cache Valley on $PM_{2.5}$ formation in Salt Lake Valley was not significant during

30 the study period. As shown in Fig. S16, the transport of NH_3 from Cache County and Franklin County into the medium densely populated North Metropolitan area (Weber County and Davis County) was also minor (<2%) during PCAP periods. Segregating the contributions from each county by emission sector, we found that 55 % are from area emissions and about

30 % from mobile sources (Fig. S18). If we account for the observed underestimation of emission sources in the UDAQ inventory by increasing area source and mobile emissions by a factor 4.5 and 3, respectively, (Fig. S19) and take the average values retrieved from the Twin Otter and the UU site, during the study period about 60 % of dNH_x in Salt Lake Valley originated from area source and 30 % from mobile source emissions in the region. Future analyses of relationships between

5 NH_3 and tracers for different emission sources, such as CO, CO_2, CH_4, NO_x and VOCs, will be useful in refining the apportionment of NH_3 emission sources from this campaign.

For Cache Valley, during PCAP conditions 64.2% of dNH_x contributions were from Cache Valley, while 21.1% were transported from Box Elder County which is connected through a canyon in the west mountain range of Cache Valley. Due to excess NH_3 in Cache Valley, ammonium nitrate formation is mostly nitrate-limited (Franchin et al., 2018). Therefore, the

10 advection of nitrate or NO_x may be a significant process for $PM_{2.5}$ formation in Cache Valley. Figure 8b, shows the percentage of county contributions for dNO_y (for all regions see Fig. S17). As they are based on the same STILT footprints, percentages are similar to the dNH_x contributions, but differ due to a different distribution of NO_x emission sources. During PCAP conditions, 19.5% of dNO_y in Cache Valley was emitted in Box Elder County, 16.8% in Davis County, 13.0% in Weber County, and 11% in Salt Lake County. This suggests that a large fraction of NO_x potentially leading to $PM_{2.5}$ formation in

15 Cache Valley may not be locally emitted but mixed in from other counties.

For Utah Valley, inter-valley exchange seems slightly less important than for Cache Valley as 58.7% of dNH_x and 57.6% of dNO_y originated in Utah County during PCAP periods. Nonetheless, transport from Salt Lake County during PCAP conditions is still significant with contributions of 17.5% to dNH_x and 29.9% to dNO_y. During non-PCAP conditions the percentage contributions from Salt Lake County to dNH_x (29.9%) and dNO_y (49.8%) are even higher, although formation of NH_3NO_4 is

20 less important as demonstrated in lower $PM_{2.5}$ levels observed (Fig. 3).

4 Conclusions

Winter air pollution in the Great Salt Lake Region has been shown to be mainly linked to the formation of ammonium nitrate aerosol. Understanding the sources of NH_3 is key to making reliable predictions of ammonium-aerosol formation and identifying the appropriate mitigation strategies for $PM_{2.5}$. To investigate NH_3 emissions in the Great Salt Lake Region, we

25 sampled NH_3 and pNH_4 from a Twin Otter aircraft over the Great Salt Lake Region in Northern Utah and at selected ground sites

We found that NH_x (= NH_3+pNH_4) was highest in Cache Valley, which can be attributed to the large number of NH_3 emitting livestock and poultry operations in the Cache Valley. However, NH_3 emissions in the commonly used UDAQ NH_3 emission inventory are not significantly larger in Cache Valley than in Salt Lake Valley or Utah Valley, as the measurements would

30 suggest. Using a STILT footprint model approach, our results suggest that in Cache Valley livestock emissions in the UDAQ

inventory are underestimated by a factor of approximately 4.5 for January and February 2017, based on the following findings: (1) the factor between modelled and measured NH_x enhancements was 4.4, and (2) total UDAQ NH_3 emissions in Cache Valley are lower by a factor of 2.61 compared to emissions estimated in the USU inventory. One reason for the discrepancy could be the underestimation of wintertime emissions through the applied monthly profile in the UDAQ emission inventory.

5 This emphasizes the importance of generating year-specific emission factors and temporal profiles that are based on the meteorological conditions of the year for which the inventory is run. Furthermore, our results suggest that in areas with large livestock operations, moving towards facility based inventories for livestock NH_3 emissions can yield better NH_3 and NH_x predictions in local or regional air quality models. However, more extensive datasets, which also include summertime measurements, would be needed to evaluate the uncertainties of livestock emissions within inventories in more detail.

10 Our investigation of the inter-valley exchange during the study period revealed that in Salt Lake Valley around two thirds of NH_x originated within the valley, while NH_x transport from Cache Valley was negligible and therefore did not significantly impact the formation of $PM_{2.5}$ in Salt Lake Valley. In contrast, transport of NH_x from Utah Valley can be significant during PCAP period when southerly winds prevail. Furthermore, we found that in Cache Valley a significant fraction (70%) of the NO_x potentially leading to $PM_{2.5}$ formation is not locally emitted and is instead transported from other counties. While nearly

15 20% of the NO_y in Cache Valley originated in the adjacent Box Elder County, still 11% of the Cache Valley NO_y was transported from Salt Lake County, about 50 km away. Since it was found that the formation of ammonium nitrate in Cache Valley was mostly nitrate limited during the UWFPS campaign, this illustrates the potential effect which regulation of NO_x emissions in Salt Lake County may have on neighbouring regions with higher agricultural NH_3 emissions.

Author contributions

20 AM performed the measurements and analysis of airborne NH_3 and wrote the manuscript. JGM provided input at all stages of the measurements, the analysis and discussion of results. AF and AMM obtained and analyzed the aircraft based AMS data. DLF, CCW and EEM obtained and analyzed the NOxCaRD data. AH and RM provided the ground site NH_3 data. AM performed the model analysis with support from AH and JCL. JCL ran the STILT model and CP, RM and KM provided the emission inventory data. SSB and MB planned and organized the UWFPS measurement campaign. All authors discussed the

25 results and contributed to the final manuscript.

Acknowledgments

The authors would like to acknowledge the Utah Division of Air Quality for their support and collaboration during the study. Specifically, NOAA acknowledges support for Twin Otter flights from the Utah Division of Air Quality under agreement number 16-049696. We thank the NOAA Aircraft Operations Center for their dedication and professionalism, particularly the pilot Robert Mitchel and Jason Clark for skillful navigation in complex terrain and challenging meteorology. We thank Bill Dube for the technical lead in installations for the instrument installations on the Twin Otter aircraft. We thank Lexie Goldberger for assistance in obtaining the presented aircraft measurements and Joel Thornton for providing input to the project design and comments to the presented manuscript. Furthermore, we would also like to thank the Utah Water Research Laboratory and the Utah State University Facilities for financial and logistical support. The data from the UWFPS campaign can be found at the NOAA website: https://www.esrl.noaa.gov/csd/groups/csd7/measurements/2017uwfps/.

References

Baek, B. H. and Seppanen, C.: Spare Modeling Operator Kerner Emissions (SMOKE) Modeling System (Version SMOKE User's Documentation), 2018.

Bahreini, R., Dunlea, E. J., Matthew, B. M., Simons, C., Docherty, K. S., DeCarlo, P. F., Jimenez, J. L., Brock, C. A. and Middlebrook, A. M.: Design and operation of a pressure-controlled inlet for airborne sampling with an aerodynamic aerosol lens, Aerosol Sci. Technol., 42(6), 465–471, doi:10.1080/02786820802178514, 2008.

Drewnick, F., Hings, S. S., DeCarlo, P., Jayne, J. T., Gonin, M., Fuhrer, K., Weimer, S., Jimenez, J. L., Demerjian, K. L., Borrmann, S. and Worsnop, D. R.: A new time-of-flight aerosol mass spectrometer (TOF-AMS) - Instrument description and first field deployment, Aerosol Sci. Technol., 39(7), 637–658, doi:10.1080/02786820500182040, 2005.

Ellis, R. a., Murphy, J. G., Pattey, E., van Haarlem, R., O'Brien, J. M. and Herndon, S. C.: Characterizing a Quantum Cascade Tunable Infrared Laser Differential Absorption Spectrometer (QC-TILDAS) for measurements of atmospheric ammonia, Atmos. Meas. Tech., 3(2), 397–406, doi:10.5194/amt-3-397-2010, 2010.

Franchin, A., Fibiger, D. L., Goldberger, L., McDuffie, E. E., Moravek, A., Womack, C. C., Crosman, E. T., Docherty, K. S., Dube, W. P., Hoch, S. W., Lee, B. H., Long, R., Murphy, J. G., Thornton, J. A., Brown, S. S., Baasandorj, M. and Middlebrook, A. M.: Airborne and ground-based observations of ammonium nitrate dominated aerosols in a shallow boundary layer during intense winter pollution episodes in northern Utah, Atmos. Chem. Phys. Discuss., 1–32, doi:10.5194/acp-2018-629, 2018.

Fuchs, H., Dubé, W. P., Lerner, B. M., Wagner, N. L., Williams, E. J. and Brown, S. S.: A sensitive and versatile detector for atmospheric NO2and NOXbased on blue diode laser cavity ring-down spectroscopy, Environ. Sci. Technol., 43(20), 7831–7836, doi:10.1021/es902067h, 2009.

Gilliland, A. B., Wyat Appel, K., Pinder, R. W. and Dennis, R. L.: Seasonal NH3emissions for the continental united states: Inverse model estimation and evaluation, Atmos. Environ., 40(26), 4986–4998, doi:10.1016/j.atmosenv.2005.12.066, 2006.

Hacker, J. M., Chen, D., Bai, M., Ewenz, C., Junkermann, W., Lieff, W., Mcmanus, B., Neininger, B., Sun, J., Coates, T., Denmead, T., Flesch, T., Mcginn, S. and Hill, J.: Using airborne technology to quantify and apportion emissions of CH 4 and NH 3 from feedlots, , (C), 190–203, 2016.

Hammond, I., S., M. R., P., S. and Baasandorj, M.: Wintertime ambient ammonia concentrations in Northern Utah's Urban

Atmospheric Chemistry and Physics
10.5194/acp-2019-266
2019-05-21
Author(s) 2019. CC BY 4.0 License.

Valleys, p. paper A53B-221, 2017 Fall meeting of the Amerian Geophysical Union, New Orleans, LA, USA, 11-15 Dec. 2017., 2017.

Jayne, J. T., Leard, D. C., Zhang, X., Davidovits, P., Smith, K. A., Kolb, C. E. and Worsnop, D. R.: Development of an aerosol mass spectrometer for size and composition analysis of submicron particles, Aerosol Sci. Technol., 33(1–2), 49–70, doi:10.1080/027868200410840, 2000.

Kelly, K. E., Kotchenruther, R., Kuprov, R. and Silcox, G. D.: Receptor model source attributions for Utah's Salt Lake City airshed and the impacts of wintertime secondary ammonium nitrate and ammonium chloride aerosol, J. Air Waste Manag. Assoc., 63(5), 575–590, doi:10.1080/10962247.2013.774819, 2013.

Kuprov, R., Eatough, D. J., Cruickshank, T., Olson, N., Cropper, P. M. and Hansen, J. C.: Composition and secondary formation of fine particulate matter in the Salt Lake Valley: Winter 2009, J. Air Waste Manag. Assoc., 64(8), 957–969, doi:10.1080/10962247.2014.903878, 2014.

Markovic, M. Z., Vandenboer, T. C. and Murphy, J. G.: Characterization and optimization of an online system for the simultaneous measurement of atmospheric water-soluble constituents in the gas and particle phases, J. Environ. Monit., 14(7), 1872–1884, doi:10.1039/c2em00004k, 2012.

McDuffie, E. E., Womack, C., Fibiger, D. L., Dube, W. P., Franchin, A., Middlebrook, A., Goldberger, L., Lee, B. H., Thornton, J. A., Moravek, A., Murphy, J., Baasandorj, M. and Brown, S. S.: On the contribution of nocturnal heterogeneous reactive nitrogen chemistry to particulate matter formation during wintertime pollution events in Northern Utah, Atmos. Chem. Phys. Discuss., 2019, 1–32, doi:10.5194/acp-2019-200, 2019.

McQuilling, A. M. and Adams, P. J.: Semi-empirical process-based models for ammonia emissions from beef, swine, and poultry operations in the United States, Atmos. Environ., 120, 127–136, doi:10.1016/j.atmosenv.2015.08.084, 2015.

Mitchell, L. E., Crosman, E. T., Jacques, A. a., Fasoli, B., Leclair-Marzolf, L., Horel, J., Bowling, D. R., Ehleringer, J. R. and Lin, J. C.: Monitoring of greenhouse gases and pollutants across an urban area using a light-rail public transit platform, Atmos. Environ., 187(May), 9–23, doi:10.1016/j.atmosenv.2018.05.044, 2018.

Moore, K. D.: Derivation of agricultural gas-phase ammonia emissions and application to the Cache Valley, Utah State University, Logan, UT., 2007.

Pozzer, A., Tsimpidi, A. P., Karydis, V. a., de Meij, A. and Lelieveld, J.: Impact of agricultural emission reductions on fine particulate matter and public health, Atmos. Chem. Phys. Discuss., 1–19, doi:10.5194/acp-2017-390, 2017.

Silcox, G. D., Kelly, K. E., Crosman, E. T., Whiteman, C. D. and Allen, B. L.: Wintertime PM2.5 concentrations during persistent, multi-day cold-air pools in a mountain valley, Atmos. Environ., 46, 17–24, doi:10.1016/j.atmosenv.2011.10.041, 2012.

Skamarock, W. C. and Klemp, J. B.: A time-split nonhydrostatic atmospheric model for weather research and forecasting applications, J. Comput. Phys., 227(7), 3465–3485, doi:10.1016/j.jcp.2007.01.037, 2008.

UWFPS: 2017 Utah Winter Fine Particulate Study Final Report ; submitted to the Utah Division of Air Quality (UDAQ). [online] Available from: https://documents.deq.utah.gov/air-quality/planning/technical-analysis/research/northern-utah-airpollution/utah-winter-fine-particulate-study/DAQ-2018-004037.pdf, 2018.

Washenfelder, R. A., Wagner, N. L., Dube, W. P. and Brown, S. S.: Measurement of atmospheric ozone by cavity ring-down spectroscopy, Environ. Sci. Technol., 45(7), 2938–2944, doi:10.1021/es103340u, 2011.

Whiteman, C. D., Hoch, S. W., Horel, J. D. and Charland, A.: Relationship between particulate air pollution and meteorological variables in Utah's Salt Lake Valley, Atmos. Environ., 94, 742–753, doi:10.1016/j.atmosenv.2014.06.012, 2014.

Wild, R. J., Edwards, P. M., Dubé, W. P., Baumann, K., Edgerton, E. S., Quinn, P. K., Roberts, J. M., Rollins, A. W., Veres, P. R., Warneke, C., Williams, E. J., Yuan, B. and Brown, S. S.: A measurement of total reactive nitrogen, NOy, together with

NO2, NO, and O3via cavity ring-down spectroscopy, Environ. Sci. Technol., 48(16), 9609–9615, doi:10.1021/es501896w, 2014.

Womack, C. C., McDuffie, E. E., Edwards, P. M., Bares, R., Gouw, J. A. de, Docherty, K. S., Dubé, W. P., Fibiger, D. A., Franchin, A., Gilman, J. B., Goldberger, L., Lee, B. H., Lin, J. C., Long, R., Middlebrook, A. M., Millet, D. B., Moravek, A., Murphy, J. G., Quinn, P. K., Riede, T. P. and Brown, S. S.: An odd oxygen framework for wintertime ammonium nitrate aerosol pollution in urban areas: NOx and VOC control as mitigation strategies, Geophys. Res. Lett., submitted, 2019.

Zhao, Z. Q., Bai, Z. H., Winiwarter, W., Kiesewetter, G., Heyes, C. and Ma, L.: Mitigating ammonia emission from agriculture reduces PM2.5pollution in the Hai River Basin in China, Sci. Total Environ., 609, 1152–1160, doi:10.1016/j.scitotenv.2017.07.240, 2017.

WHO, 2016, Ambient (outdoor) air quality and health, http://www.who.int/mediacentre/factsheets/fs313/en/

Tables

Table 1: NH₃ emission estimates and measurements by region. Data include: (1) Total NH₃ emission estimates and their sector-based proportion from the UDAQ emission inventory; (2) NH₃ emission estimates for Cache Valley from the USU emission inventory; (3) measured and modelled NHₓ mixing ratios (mean + standard deviation); (4) the ratio between measured and modelled NHₓ mixing ratios (scaling factor). The regions are: BV = Bear valley (Box Elder County); CV = Cache Valley (Cache County + Franklin County); GSL = Great Salt Lake (Box Elder County, Weber County, Davis County, Salt Lake County + Tooele County); NM = North Metro (Davis County + Weber County); TC = Tooele County, UV = Utah Valley (Utah County).

	NH$_3$ emission estimates						Mixing ratios		Scaling factor
	UDAQ					USU	Twin Otter	Model	
Region	total	area	mobile	non-road	point	total	NH$_x$ (meas)	NH$_3$ (model)	NH$_x$ meas ÷ NH$_3$ model
	kg d^{-1}	%	%	%	%	kg d^{-1}	ppbv	ppbv	mean (median)
BV	3514	97.2	2.5	0.0	0.3	-	4.09 (± 4.09)	0.82 (± 0.95)	5.0 (6.3)
CV	4757	96.7	2.9	0.0	0.4	12435	7.50 (± 9.65)	1.70 (± 1.47)	4.4 (2.7)
GSL	-	-	-	-	-	-	4.47 (± 4.68)	0.63 (± 0.96)	7.1 (12.2)
NM	2218	58.8	21.5	0.3	19.4	-	10.04 (± 8.77)	2.00 (± 2.06)	5.0 (4.7)
SLV	2016	34.4	49.3	0.6	15.7	-	3.61 (± 4.01)	1.87 (± 2.30)	1.9 (1.9)
TC	1486	92.7	6.2	0.0	1.1	-	2.78 (± 3.21)	0.33 (± 0.49)	8.4 (10.7)
UV	6058	85.5	7.2	0.1	7.2	-	3.78 (± 4.15)	2.33 (± 1.94)	1.6 (1.2)

Figures
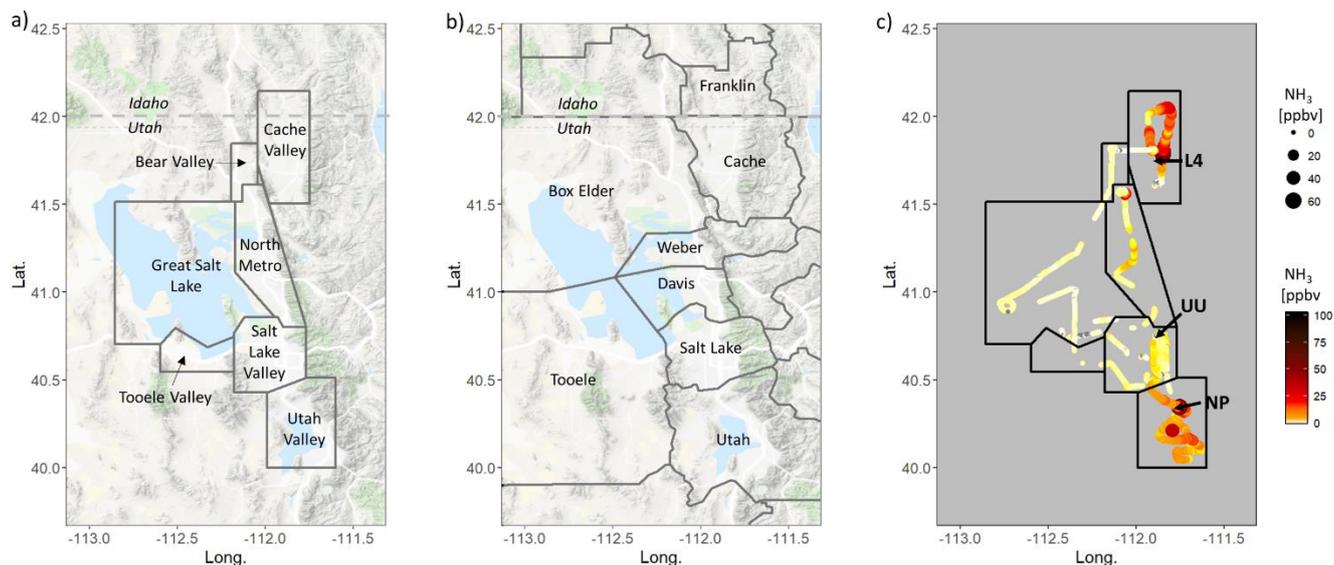
Figure 1: Overview of the study area: a) outlines of sub-regions used for the analysis of Twin Otter measurements, b) borders of counties which are part of the study area, and c) typical NH₃ mixing ratios measured from the Twin Otter combined from a north and south flight leg flight on 17 and 18 January, respectively. Arrows in c) indicate the location of ground site measurements used for this study in North Provo (NP), at the University of Utah (UU) and in Logan (L4). Borders of the sub-regions are shown in c) for reference. Salt Lake City, the most populated area, is situated in the North Eastern part of Salt Lake Valley.
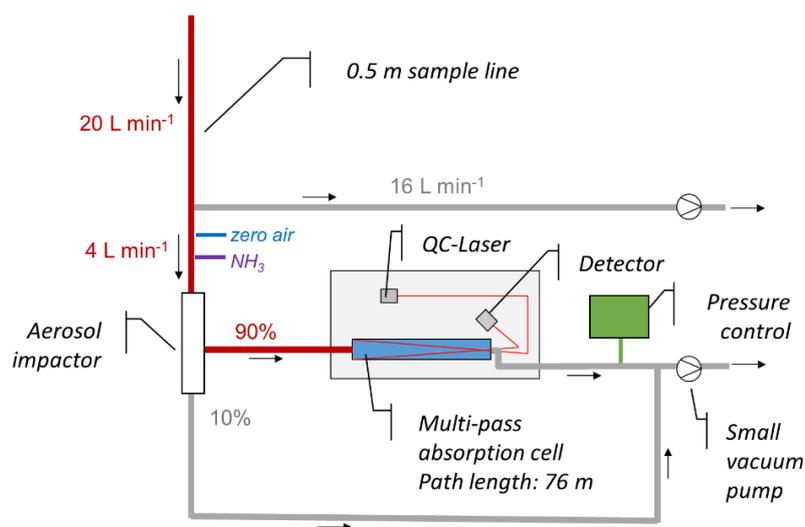
Figure 2: Setup of the QC-TILDAS on the Twin Otter aircraft for NH₃ measurements at 1 Hz sample frequency. The commercially available QC-TILDAS was modified using a smaller vacuum pump, a pressure controller and a custom made PFA aerosol impactor. A bypass system was used to generate a higher flow rate through the inlet line. See text for a detailed description of the setup.
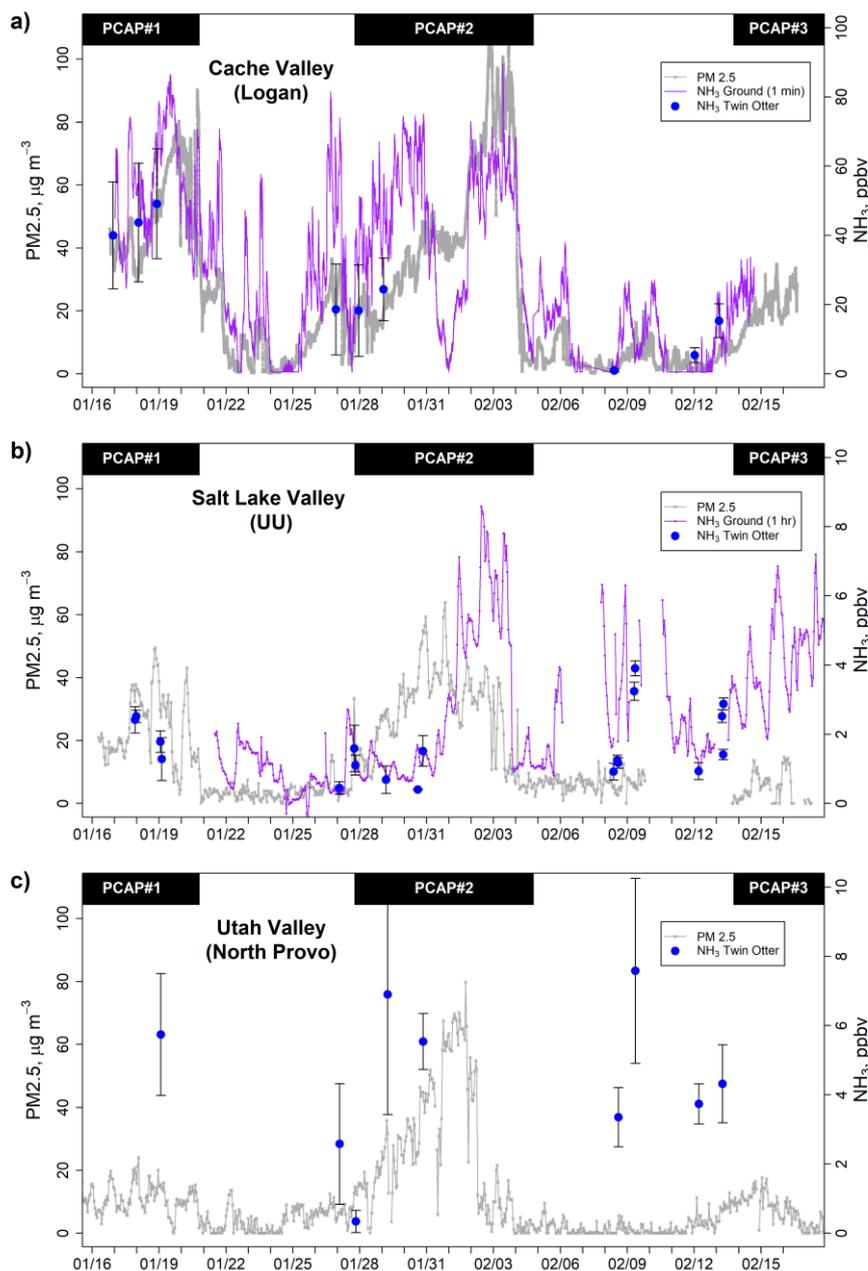
Figure 3: Time series of fine particulate matter ($PM_{2.5}$) and NH_3 mixing ratios during PCAP periods over the course of the measurement campaign from Jan 16 to Feb 13 2017. Shown are measurements from the ground sites (a) at the University of Utah (UU), (b) in Logan (L4), and (c) in North Provo (NP). Blue dots represent mean NH_3 mixing ratios measured from the Twin Otter during missed approaches (at Logan airport and North Provo airport) or when flying over the UU measurement site. The time frames of the three PCAP periods during the campaign are marked as black bars.
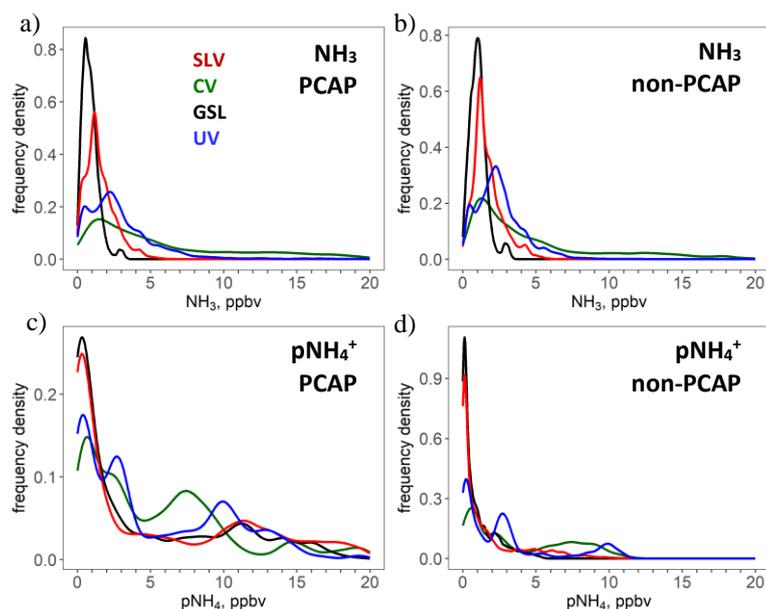
Figure 4: Frequency distribution of NH₃ (a, b) and pNH₄ (c, d) mixing ratios measured from the Twin Otter in Salt Lake Valley (SLV), Cache Valley (CV), Utah Valley (UV) and above the Great Salt Lake (GSL). The distributions are based on mixing ratios from all research flights, segregated into PCAP (a, c) and non-PCAP (b, d) conditions.
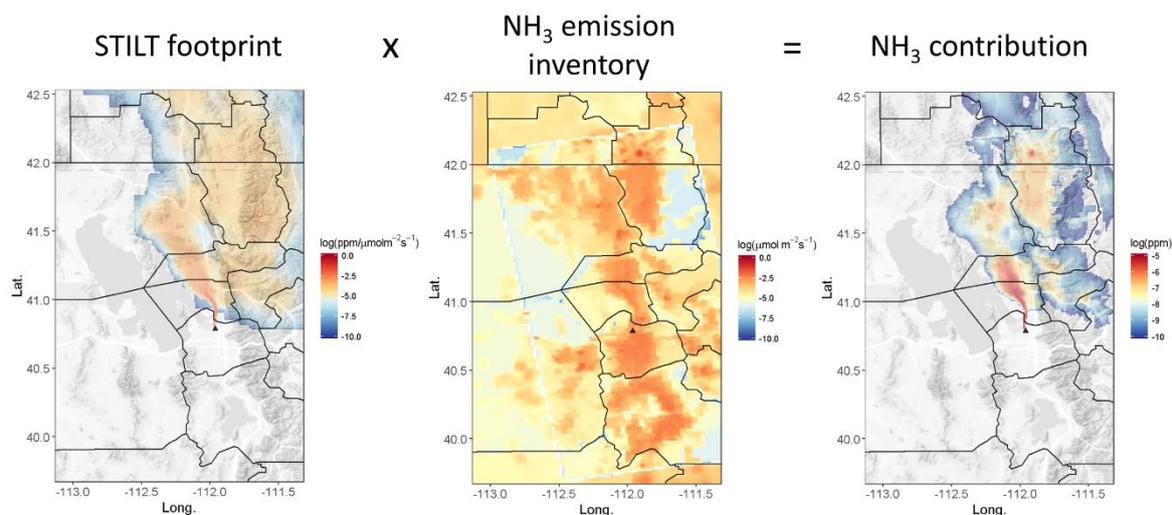
Figure 5: Approach used to determine NH₃ enhancements by overlaying the emission sensitivity map (in ppmv/(μmol m⁻² s⁻¹), left panel) with the NH₃ emissions from the UDAQ emission inventory (in μmol m⁻² s⁻¹, centre panel). The emission sensitivities were derived with STILT for every 2 min of the Twin Otter flight path for all research flights. NH₃ enhancement for the Twin Otter location were obtained by summing of all NH₃ contributions within the spatial domain of the NH₃ contribution map. The NH₃ Emission inventory map (centre panel) is a composite of the 1.33 x 1.33 km² resolution emission inventory in the centre, imbedded into the 4 x 4 km² emission inventory.
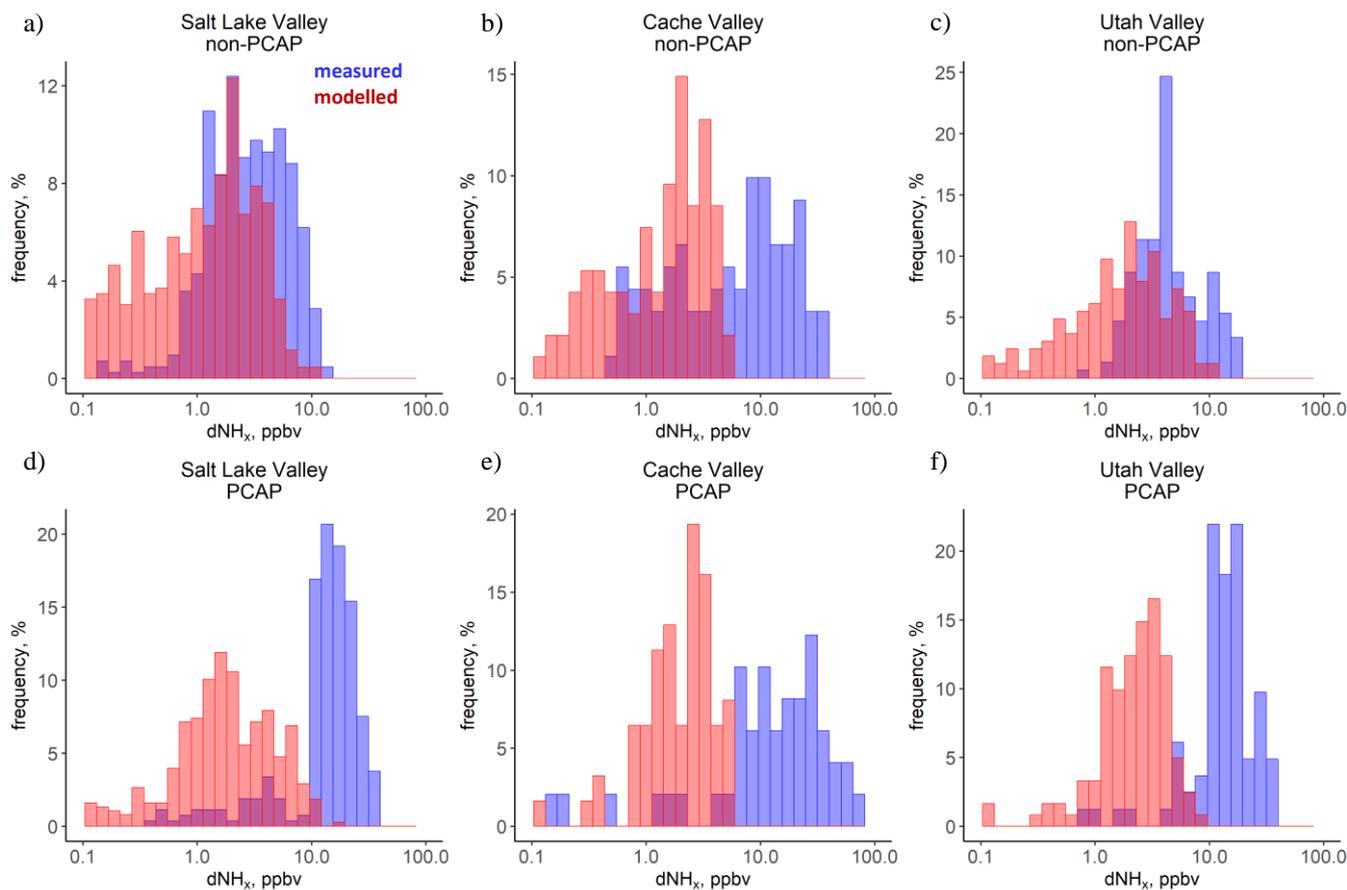
Figure 6: Frequency distribution of measured (blue) and modelled (red) NH$_x$ enhancements (dNH$_x$) for Salt Lake Valley, Cache Valley and Utah Valley on logarithmic scales for (a-c) non-PCAP and (d-f) PCAP conditions.
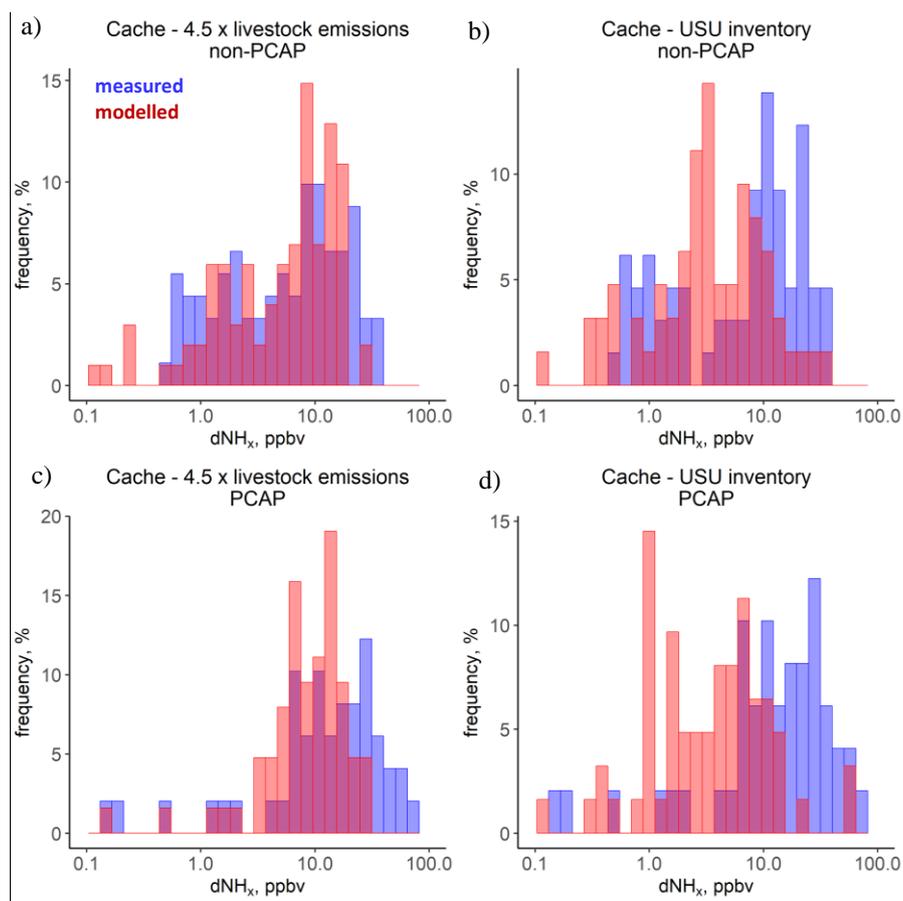
Figure 7: Frequency distribution of measured (blue) and modelled (red) NH$_x$ enhancements (dNH$_x$) for Cache Valley, using enhanced livestock emissions by a factor of 4.5 and the USU emission inventory for (a+b) non-PCAP and (c+d) PCAP conditions.
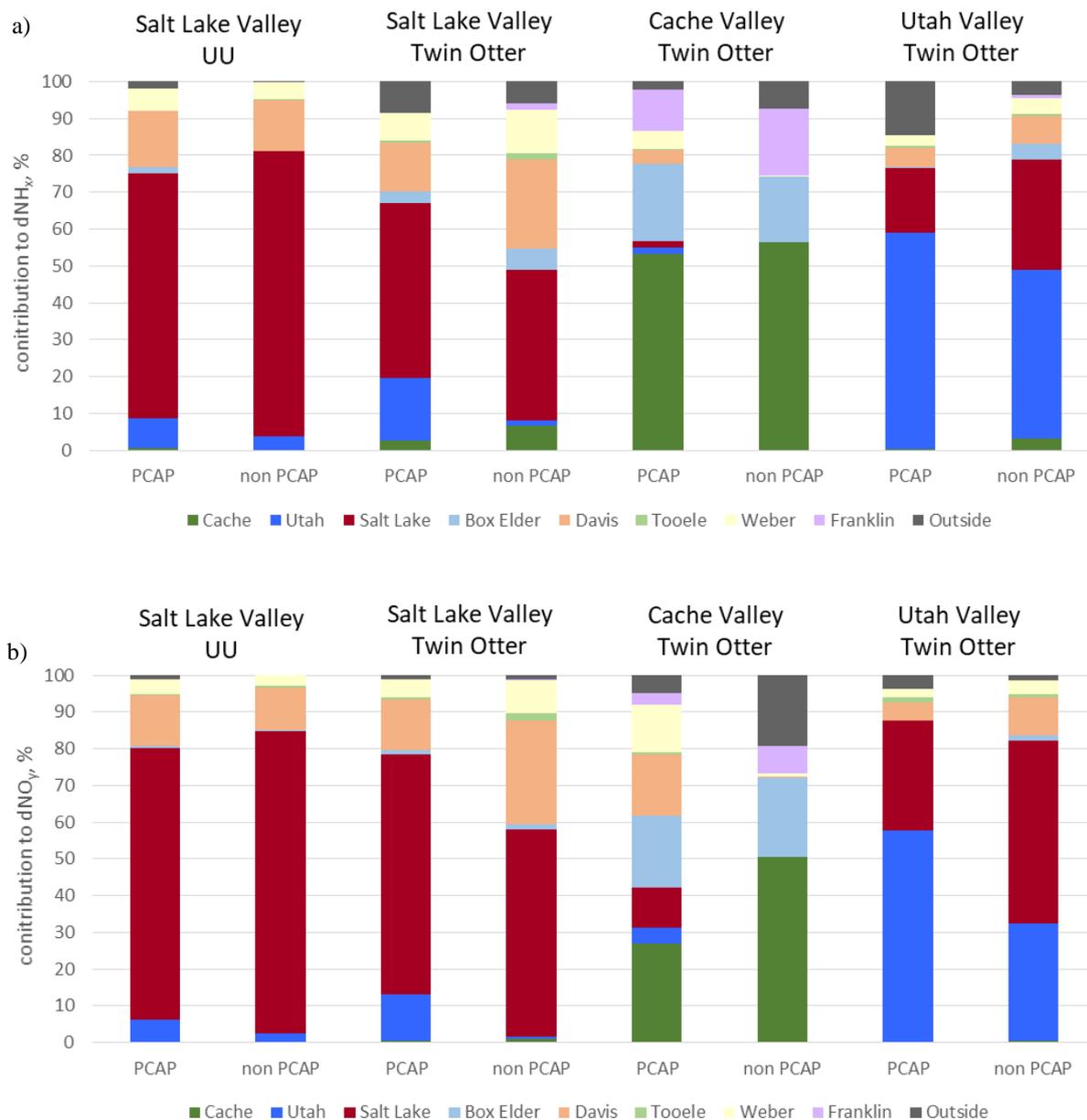
Figure 8: Inter-valley exchange of pollutants: Contributions from different counties to (a) dNH$_x$ and (b) dNO$_y$ at the UU (Salt Lake Valley) site and Twin Otter locations in Salt Lake Valley, Cache Valley and Utah Valley. The inter-valley exchange was evaluated by segregating contributions from the footprint model (see contributions map in Figure 5) into counties of origin for each run of the footprint model (i.e. every 2 min of Twin Otter flight path, and every hour for UU location).